EFDA–JET–CP(08)03-03

D.C. McDonald, L. Laborde, J.C. DeBoo, F. Ryter, M. Brix, C.D. Challis,
P. de Vries, C. Giroud, J. Hobirk, D. Howell, E. Joffrin, T.C. Luce,
J. Mailloux, V. Pericoli-Ridolfini, A.C.C. Sips, K. Thomse
and JET EFDA contributors

JET Confinement Studies and their Scaling to High β_N, ITER Scenarios

JET Confinement Studies and their Scaling to High β_N, ITER Scenarios

D.C. McDonald[1], L. Laborde[1], J.C. DeBoo[2], F. Ryter[3], M. Brix[1], C.D. Challis[1], P. de Vries[1], C. Giroud[1], J. Hobirk[3], D. Howell[1], E. Joffrin[4], T.C. Luce[2], J. Mailloux[1], V. Pericoli-Ridolfini[5], A.C.C. Sips[3], K. Thomsen[6] and JET EFDA contributors*

JET-EFDA, Culham Science Centre, OX14 3DB, Abingdon, UK

[1]EURATOM-UKAEA Fusion Association, Culham Science Centre, OX14 3DB, Abingdon, OXON, UK
[2]General Atomics, P O Box 85608, San Diego, California 92186-5608, USA
[3]Max Planck-Institute fur Plasmaphysik, EURATOM Association, D-85748 Garching, Germany
[4] Association Euratom-CEA, CEA Cadarache, F-13108, St Paul lez Durance, France
[5]Associazione Euratom-ENEA sulla Fusione, C R Frascati, C P 65, 00044-Frascati, Italy
[6]EFDA Close Support Unit, D-85740 Garching, Germany
** See annex of M.L. Watkins et al, "Overview of JET Results ", (Proc. 21 st IAEA Fusion Energy Conference, Chengdu, China (2006)).*

Preprint of Paper to be submitted for publication in Proceedings of the 35th EPS Conference on Plasma Physics, Hersonissos, Crete, Greece (9th June 2008 - 13th June 2008)

ABSTRACT.
The ITER Hybrid scenario aims to exploit bootstrap current to enable burn times in excess of 1000s. To achieve this, and optimise fusion performance, requires high β_N (the plasma pressure normalised to a stability scaling) and energy confinement equal to or greater than that predicted for the baseline scenario. This paper discusses results from the JET candidate Hybrid scenario, where $\beta_{N,MHD} \leq 3.6$ plasmas have been produced. Despite a different initial phase, confinement relevant plasma parameters evolve rapidly towards those of equivalent ELMy H-modes and are well described by IPB98(y,2). In contrast to previous ELMy H-mode studies, a dedicated β scan experiment in the JET Hybrid candidate scenario shows a strong negative dependence of global confinement on β_N. Analysis indicates that the core transport remains consistent with weakly dependent electrostatic transport, whilst the edge confinement decreases strongly with increasing β_N. By combining global confinement data from ASDEX Upgrade, DIII-D and JET Hybrid scenario discharges, a multi-machine database is produced. In contrast to the JET case, confinement in ASDEX Upgrade and DIII-D is is shown to be inconsistent with IPB98(y,2) and alternative dependencies are explored.

1. INTRODUCTION

By operating at high β_N, the ITER Hybrid scenario aims to exploit bootstrap current to enable burn times in excess of 1000s [1, 2]. Here, $\beta_N = c_0 \beta aB/I$ is the plasma $\beta = 2\mu_0 \langle p \rangle / B^2$ normalised to a stability scaling, $c_0 = 10^8 m^{-1} 1TA^{-1}$, a is the plasma minor radius, B is the vacuum magnetic field, I is the plasma current, μ_0 is the permeability of vacuum, and $\langle p \rangle$ is the volume averaged plasma pressure [3]. To achieve this, and optimise fusion performance, these scenarios must have good energy confinement [4]. ELMy H-mode plasma studies, with β_N's primarily in the range $1 < \beta_N < 2$, have produced scalings, such as IPB98(y,2) [5], which describe the confinement time, τ_E, in existing experiments reasonably well and are used for extrapolation to ITER [6, 7]. Expressed in dimensionless parameters [8, 3], the IPB98(y,2) confinement time scaling, $\tau_{98(y,2)}$, has a scaling of $\omega_{ci}\tau_{98(y,2)} \propto \beta^{-0.9}$ [9], where ω_{ci} is the ion Larmor gyro-frequency. Such a strongly negative scaling is in contrast to that predicted by plasma transport models dominated by electrostatic turbulence, which predict almost β independent transport [3]. However, dedicated ELMy H-mode β scan studies, in which β is varied whilst the other important dimensionless parameters are kept constant [3], in JET [10] and DIII-D [11] found almost no dependence of normalised confinement on β. As well as being consistent with electrostatic transport, these ELMY H-mode results support β independent scalings, such as the electrostatic gyroBohm scaling [9], which predict higher confinement and performance for ITER at high β_N [11]. However, subsequent studies at JT-60U [12] and ASDEX Upgrade [13] did find a negative dependence of normalised confinement on β, although somewhat weaker than that of IPB98(y,2). Overall, these results show a range of β scalings and the physics basis for energy confinement at high β_N clearly needs improving before existing confinement scalings can be extrapolated to high β_N with any confidence. With this aim, this paper reports the results from and analysis of a dedicated β scan performed in JET in a scenario compatible with high β_N operation.

High performance, high β_N discharges in JET are achieved by using a scenario which includes a rapid increase of the plasma current prior to the main heating phase designed to give a broad q-profile [14]. This is intended to stabilise potentially disruptive MHD activity and so enable access to high β_N operation. In this paper, such a scenario will be referred to as the JET Hybrid scenario. This scenario is a candidate for the ITER Hybrid scenario. Similar scenarios have been developed to achieve high performance, high β discharges in DIII-D [15, 16] and ASDEX Upgrade (improved H-mode, [17]) and will also be referred to here as Hybrid scenarios. This paper focuses on these scenarios, which at present provide the most promising candidates for ITER Hybrid operation. JET Hybrid studies have covered a range of configurations, currents (1.1-2.8MA), fields (1.3-3.5T) and $\beta_{N,MHD} \leq 3.6$. Here, $\beta_{N,MHD}$ is a measure of β_N taken from the MHD equilibrium reconstruction. Despite a different initial phase, plasma parameters evolve rapidly (≈1*s*) towards those of equivalent ELMy H-modes [18] and their τ_E is well described by IPB98(y,2) [14]. In contrast, ASDEX Upgrade and DIII-D Hybrid scenarios observed confinement times significantly above IPB98(y,2) with $H_{98(y,2)} = \tau_E/\tau_{98(y,2)}$ up to 1.7-2.0 for ASDEX Upgrade [19, 17] and 1.7-1.8 for DIII-D [15, 16]. Thus, the Hybrid scenario is a promising candidate for ITER Hybrid operation as it has achieved τ_E equal to or greater than equivalent H-modes on all three machines. However, the differences between these confinement times and the IPB98(y,2) scaling in ASDEX Upgrade and DIII-D mean that it is not clear how to extrapolate the performance of existing Hybrid scenarios to ITER.

The rest of this paper is organised as follows: section 2 describes the β scan performed in the JET Hybrid scenario. Section 3 describes studies of a global confinement database comprising discharges from JET, ASDEX Upgrade and DIII-D. Section 4 provides a summary of the results and conclusions.

2. BETA SCAN IN JET HYBRID SCENARIO

2.1. EXPERIMENTAL SET-UP

The experimental procedure is similar to that for the ELMy H-mode β scans [10], except that the discharges were performed in the JET candidate Hybrid scenario of Section 1 in a high triangularity, $\delta = 0.45$, configuration. The discharges were heated with Neutral Beam Injection (NBI) heating only and fuelled with deuterium gas injection. Three different magnetic fields, *B*, were used and, for each one, the plasma current, NBI heating and gas fuelling were adjusted so as to match the dimensionless parameters q_{95} and the global ρ^* and ν^* [7] between the three discharges. Here q_{95} is the safety factor on the magnetic surface containing 95% of the flux of the last closed flux surface, ρ^* is the normalised ion Larmor radius, and ν^* is the normalised ion-electron collisionality. Unlike the ELMy H-mode scans, the NBI tuning was performed using real-time feedback on the plasma energy. This resulted in a scan over $\beta_{N,MHD} = 1.7-2.7$, $\beta_{N,th} = 1.5-2.0$. Diagnosis was as for the ELMy H-mode β scans [10], except that equilibria were computed by the EFIT code [20] constrained by magnetics and a motional Stark effect diagnostic [21].

2.2. EXPERIMENTAL RESULTS

Figure 1(a) shows time traces for the three discharges produced. Matching of ρ^* and ν^* requires matched density, normalised as n/B^4, and temperature, normalised as T/B^2, [3]. These parameters can be seen to agree within errors, except for the density in the low β discharge which is ≈8% too high. q_{95} is well matched. All discharges had regular Type I ELMs with frequency, f_{ELM}, increasing with increasing β. Profile plots, figure 1(b), show the majority of the data for ρ^* agrees at the 10% level and for ν^* at the 20% level. q-profiles are in good agreement, but with a somewhat broader profile for the low $\beta_{N,th}$ = 1.5 discharge. The ratio of ion to electron temperature and Z-effective agree well with each other within errors. The normalised toroidal ion Mach numbers, M_{tor}, agree well at the core but the profile for the high $\beta_{N,th}$ = 2.0 discharge is more peaked. No (3,2) neoclassical tearing mode (NTM) or MARFE activity, known to affect confinement in JET [22, 10] was observed. (4,3) NTM activity was observed in all discharges.

Figure 2(a) shows the normalised confinement, $B\tau_E \propto \omega_{ci}\tau_E$, plotted against β_N calculated for the thermal components only, $\beta_{N,th}$. This measure of β_N is the most relevant to thermal energy confinement. A clear trend of decreasing normalised confinement with increasing $\beta_{N,th}$ is observed. A best fit log-linear scaling of $B\tau_E \propto \beta_{N,th}^{-1.40\pm0.38}$ well represents these measurements. Such a dependence contrasts strongly with the negligible $\beta_{N,th}$ dependence observed in previous experiments on JET [10] and in DIII-D [11] and is considerably stronger than the negative dependencies of normalised confinement on $\beta_{N,th}$ observed in experiments on JT-60U [12] and ASDEX Upgrade [13]. The observed dependency is also stronger than the $\tau_E \propto \beta_{N,th}^{-0.9}$ scaling of IPB98(y,2).

To assess the relative impacts of core transport and the Edge Transport Barrier (ETB), the confinement was separated into core and edge measurements. The regions were separated at a normalised square root toroidal flux, x, of 0.8 which lies just inside of the ETB. The energy confined outside of x = 0.8, which includes all of that in the ETB, and the energy confined inside of x = 0.8, which includes the bulk of the core confinement, were taken from the experimental data using the method given in Ref. [23]. Dividing these energies by the loss power gives an effective confinement for the inner and outer regions. Figure 2(b) shows the normalised effective confinement for these two regions plotted against $\beta_{N,th}$. Across the scan, normalised confinement decreases with increasing $\beta_{N,th}$ by 61% in the outer region and by 44% in the inner region. This provides strong evidence that the energy confinement in the ETB is decreasing with increasing $\beta_{N,th}$ as predicted by models where the ETB pressure is constrained by MHD stability [24].

An interpretative analysis of core transport was performed using the TRANSP code [25, 26]. Results show strongly coupled ion and electron channels. As a result, the ion, χ_i, and particularly the electron, χ_e, thermal conductivities are difficult to separate outside of the experimental error bars. However, it does appear that thermal transport is predominantly in the ion channel. Local transport is instead expressed in terms of the local effective thermal conductivity, $\chi_{eff} = (n_e\chi_e + n_i\chi_i)/(n_e + n_i)$, where n_i and n_e are the ion and electron densities respectively. Figure 3(a) shows the profile for the normalised effective thermal conductivity, $\chi_{eff}/(\omega_{ci}a^2) / \chi_{eff}/B$ [3], for the region x =

0.3–0.7. The analysis is adversely affected by the transient effects of sawteeth for $x < 0.3$ and ELM losses for $x > 0.7$. χ_{eff} confidence intervals are estimated from the spread in the derived χ_{eff} over a one second window. The normalised χ_{eff} is observed to increase with increasing $\beta_{N,th}$ for the bulk of the region $x = 0.3$–0.7. This behaviour is qualitatively consistent with the confinement analyses already discussed, but contrasts with the results from the previous JET β studies [10, 27].

2.3. COMPARISON WITH GYRO-FLUID TRANSPORT MODELS

The core transport for the experiments of this section has been compared with gyro-fluid transport models [28]. Both the Weiland model [29] and Gyro-Landau-Fluid model (GLF23) [30] were given input data (equilibrium, B, I, n_i, n_e, Z-effective and M_{tor} profiles and the thermal boundary condition at $x = 0.8$) and then run to predict the ion and electron thermal profiles. Data from the central point of the β scan experiment were taken as input data and numerical β scans were performed by scaling the input parameters as for a β scan. For each point in the scan, P was adjusted to match ρ^* and ν^*. As observed in previous gyro-fluid [31, 32] and gyro-kinetic [33, 34, 35] simulations, a weak dependence of transport on β_N is observed. Figure 3(b) shows the normalised confinement time over a region from $x = 0$–0.8 taken from the experimental data (diamonds) and from such an ideal scan with the Weiland model (asterisks). Normalised confinement in the modelled "ideal" scan clearly has a weaker dependence on β_N than the experiments and also has the wrong direction. The modelling was then repeated using the experimental measurements for each individual point in the scan with the small differences in the normalised parameters and boundary conditions. These simulations differed markedly from the "ideal" scan simulations and showed much better agreement with the experimental data. These results, for the case of the Weiland model, are shown as circles in figure 3(b). This modelling predicts both the direction and magnitude of the β_N dependency within the experimental errors.

These studies show that the strong confinement decrease with increasing β_N observed in the JET experiments is compatible with existing electrostatic core transport models that predict a very weak dependence of transport on β_N. The observed β_N dependence can be explained by small differences in parameters and boundary conditions. The decrease in normalised ETB confinement with increasing $\beta_{N,th}$, discussed in Section 2.2, results in different core boundary conditions and this alone may be responsible for the observed core dependence and resulting global scaling. Analysis of the full JET dataset of improved confinement shows some evidence for a weak dependence of confinement on $\beta_{N,th}$ at low triangularity, $\delta < 0.3$ and a stronger negative dependence at high triangularity $\delta > 0.3$. This is consistent with the results of the experiments presented here, where $\delta = 0.45$, and previous JET ELMy H-mode studies [10], where $\delta = 0.2$. Multi-machine studies have also indicated a sensitivity of the β scaling of confinement to shape, but with a more subtle from than a simple δ [36]. The MHD stability of the ETB has been shown to be sensitive to shape [37] and this offers a likely mechanism for the observed differences in scaling. Experimental demonstration of this requires detailed analysis of the ETB profiles, the data for which were not available for the current experiments, and so must await future studies.

3. MULTI-MACHINE GLOBAL CONFINEMENT ANALYSIS

As discussed in Section 1, the extrapolation of the confinement times from the existing Hybrid scenarios in various tokamaks to ITER requires the development of a physics basis common to them all. With this aim, a global confinement dataset was constructed comprised of a large number of Hybrid scenario discharges from ASDEX Upgrade [19, 17], DIII-D [15, 16] and JET [14]. The number of data points, *N*, and the ranges of key parameters in the dataset for each machine are given in table 1.

For DIII-D, *B* field and *I* are relatively fixed, mostly at 1.2*MA* and 1.7*T*, but cover a wide range for the other machines. A wide range of line average electron densities, $\bar{n}_e$, and *P* are covered for each machine. Discharges with $\beta_{N,MHD}$ up to 3.5 are included from all machines, although the maximum $\beta_{N,th}$ are somewhat lower. Because of its larger size, JET has the highest τ_E in the dataset, but its H-factors are lower than for the other machines.

Figure 4(a) shows the confinement times for the discharges in this dataset plotted against the IPB98(y,2) scaling. Data from the ITER-like DB3 dataset of ELMy Hmodes taken from the H-mode confinement database [7] are also shown. The JET data are in agreement with the IPB98(y,2) scaling and lie within the ELMy H-mode dataset. The ASDEX Upgrade and DIII-D Hybrid data lie above the IPB98(y,2) scaling and largely outside of the ELMy H-mode data. Data from both machines show systematic trends with the highest deviation from $\tau_{98(y,2)}$ associated with higher confinement. This indicates that data from these machines contain a different parametric dependence to $\tau_{98(y,2)}$ and so confinement can not be extrapolated using this scaling or a form like $H_{98(y,2)} = c$, where *c* is a constant.

For the DIII-D data, $\bar{n}_e$ and *P* are the only parameters in the IPB98(y,2) scaling that vary over a considerable range and this subset of data is reasonably conditioned for a log-linear fit of τ_E to these two parameters. The resulting scaling is $\tau_E / \bar{n}_e^{0.31\pm0.04} P^{-1.03\pm0.04}$ which has a significantly stronger power scaling than $\tau_{98(y,2)}/\bar{n}_e^{0.41}P^{-0.69}$. The DIII-D Hybrid scenario discharges were produced using feedback control on auxiliary heating to maintain the required $\beta_{N,MHD}$. If there were no variation in $\beta_{N,MHD}$, such a system would fix the thermal energy as *P* varied and so force a scaling of $\tau_E \propto P^{-1}$. There is some variation in $\beta_{N,MHD}$ in the DIII-D dataset but it is rather small, ±0.5 about a mean value of 2.7. Even allowing for such a bias, it appears that the power dependence in the DIII-D data is more strongly negative than for $\tau_{98(y,2)}$. Restricting the ASDEX Upgrade dataset to $I = 1MA$ gives an equally well conditioned dataset with a fitted $\tau_E \propto \bar{n}_e^{0.39\pm0.04} P^{-0.94\pm0.03}$, similar to that of DIII-D.

The full three machine dataset is insufficiently well conditioned to perform a loglinear fit similar to IPB98(y,2). Instead, the residuals of τ_E with respect to $\tau_{98(y,2)}$ are analysed by studying the dependence of $H_{98(y,2)}$ on various parameters. If the IPB98(y,2) scaling has correct, or broadly correct, scalings for the Hybrid dataset for some of the parameters, such an analysis can be used to find the other parametric dependencies that differ. No systematic residual dependencies are observed with respect to elongation, δ, *I*, *B*, *a* or major radius. Residuals with respect to *ne* indicate some evidence of a negative $\bar{n}_e$–$H_{98(y,2)}$ correlation for the ASDEX Upgrade and DIII-D data, but no

consistent dependency between the machines. Residuals with respect to P show a clear negative $P-H_{98(y,2)}$ correlation for the DIII-D dataset, in line with the discussion above, but little sign of a $P-H_{98(y,2)}$ correlation in ASDEX Upgrade or JET. No significant correlations are found between $H_{98(y,2)}$ and β, β_N or τ_E. However, a strong positive $\rho^*-H_{98(y,2)}$ correlation is observed within the data from each machine. Where data from different machines overlaps in ρ^*-space, similar values of $H_{98(y,2)}$ are observed for each machine, figure 4(b). This would suggest that the ρ^* dependence within the Hybrid dataset is weaker than that in the gyroBohm-like, $\tau_E \propto \tau_{Bohm}/\rho^*$, IPB98(y,2) scaling. This is in line with dedicated *1/2* scans in high q_{95}, ELMy H-mode plasmas in DIII-D where confinement was observed to be Bohm-like [3]. This has been interpreted as being related to the shorter length scales of the q-profile in such discharges [3]. However, it should be noted that a residual dependence of τ_E on other variables, or groups of variables, correlated with ρ^* would also explain the behaviour seen in the figure.

SUMMARY AND DISCUSSION

Confinement studies of JET Hybrid plasmas, where q-profile evolution is modified to enable access to the high β_N operation required for the ITER hybrid scenario [1], cover a range of shapes, $I = 1.1-2.8MA$, $B = 1.3-3.5T$ and $\beta_{N,MHD} \leq 3.6$ [14, 2]. Despite a different initial phase, confinement relevant plasma parameters evolve rapidly ($\approx 1s$) towards those of equivalent ELMy H-modes. Global confinement is found to be largely in agreement with the IPB98(y,2) scaling with $H98(y,2) = 0.8-1.2$. This contrasts with previous H-mode studies on JET which indicated that confinement increased, relative to the IPB98(y,2) scaling, with increasing $\beta_{N,th}$ [10].

A β_N scan was performed with $\beta_{N,MHD} = 1.7-2.7$, $\beta_{N,th} = 1.5-2.0$. A strong de[zease in normalised confinement with increasing $\beta_{N,th}$ is observed in the core ($x < 0.8$) and edge ($x > 0.8$) regions, with the strongest decrease in the edge. The wider JET Hybrid dataset suggests that decreasing confinement with increasing $\beta_{N,th}$ is observed for configurations with $\delta \geq 0.3$. Theory based modelling of the thermal transport predicts a weak dependence of core confinement on $\beta_{N,th}$ in this parameter range, but when these models are run with the same boundary conditions and small differences in parameters as in the experiment, good agreement with experiment is observed. These results are consistent with weakly $\beta_{N,th}$ dependent core transport and confinement in the ETB being either weakly or strongly dependent on $\beta_{N,th}$ depending on the configuration.

A dataset has been produced by combining the JET dataset with ASDEX Upgrade and DIII-D Hybrid plasmas. Global confinement in this dataset is not well described by the IPB98(y,2) scaling, ASDEX Upgrade and DIII-D confinement tending to be above the scaling and to follow a different trend. $H98(y,2)$ increases with increasing ρ^* within each machine and across the multi-machine dataset. This supports the view that a confinement scaling common to these machines may be feasible, but such a scaling is unlikely to predict $H98(y,2) > 1$ at ITER-like ρ^*.

Whilst considerable progress has been made on understanding the confinement properties of high β_N discharges, no predictive empirical or theory-based model has yet been derived. Available

τ_E scalings, such as IPB98(y,2), do not well represent the existing experiments on all machines. Until strong ($H98(y,2)$ *1/4* 1.5) confinement can be demonstrated at low ρ^*, extrapolating H-factors above those of typical ELMy H-modes observed in existing experiments to predicted ITER plasmas is clearly inappropriate.

ACKNOWLEDGEMENTS

This work was funded jointly by the UK EPSRC, by the European Communities under the contract of Association between EURATOM and UKAEA, and by a EURATOM Intra-European Fellowship. The views and opinions expressed herein do not necessarily reflect those of the European Commission. This work was carried out within the EFDA framework. The work on DIII-D was supported by the US Department of Energy under DE-FC02-04ER54698.

REFERENCES

[1]. Green B.J. for the ITER International Team and Participant Teams 2003 *Plasma Physics and Controlled Fusion* **45** 687–706
[2]. Joffrin E. 2007 *Plasma Physics and Controlled Fusion* **49** B629–B649
[3]. Luce T.C. *et al.* 2008 *Plasma Physics and Controlled Fusion* 50 043001 (87pp)
[4]. Peeters A.G. *et al.* 2007 *Nuclear Fusion* **47** 1341–1345
[5]. ITER Physics Basis: Chapter 2 1999 *Nuclear Fusion* 39 2175–2249
[6]. Doyle E J *et al.* 2007 *Nuclear Fusion* **47** S18–S127
[7]. McDonald D C *et al.* 2007 *Nuclear Fusion* **47** 147–174
[8]. Kadomtsev B.B. 1995 *Sov. J. Plasma Phys* **1** 295
[9]. Petty C.C. *et al.* 2003 *Fusion Science and Technology* **43** 1
[10]. McDonald D.C. *et al.* 2004 *Plasma Physics and Controlled Fusion* **46** A215–A225
[11]. Petty C.C. *et al.* 2004 (AIP) vol. 11 pp. 2514–2522 doi:10.1063/1.1666263
[12]. Urano H. *et al.* 2006 *Nuclear Fusion* **46** 781–787
[13]. Vermare L. *et al.* 2007 *Nuclear Fusion* **47** 490–497
[14]. Joffrin E. *et al.* 2005 *Nuclear Fusion* **45** 626–634
[15]. Wade M.R. *et al.* 2005 *Nuclear Fusion* **45** 407–416
[16]. Luce T.C. for the DIII-D Team 2005 *Nuclear Fusion* 45 S86–S97
[17]. Sips A.C.C. *et al.* 2007 *Nuclear Fusion* **47** 1485–1498
[18]. Watkins M.L. on behalf of JET EFDA Contributors 2006 *Proc. 21st Fusion Energy Conference* (Chengdu, China)
[19]. Wolf R.C. *et al.* 1999 *Plasma Physics and Controlled Fusion* **41** B93–B107
[20]. Lao L.L. *et al.* 1985 *Nuclear Fusion* **25** 1611
[21]. Stratton B.C. *et al.* 1999 (AIP) vol. 70 pp. 898–901 doi:10.1063/1.1149318
[22]. Buttery R J *et al.* 2003 *Nuclear Fusion* **43** 69–83

[23]. Thomsen K *et al.* 2002 *Plasma Physics and Controlled Fusion* **44** A429–A435
[24]. Christiansen J.P. *et al.* 1998 *Nuclear Fusion* **38** 1757–1766
[25]. Goldston R.J. *et al.* 1981 *Journal of Computational Physics* **43** 61–78
[26]. Budny R.V. *et al.* 1995 *Nuclear Fusion* **35** 1497–508
[27]. Budny R.V. *et al.* 2000 *Physics of Plasmas* **7** 5038–5050 doi:10.1063/1.1320466
[28]. Laborde L. *et al.* 2008 *in preparation for Physics of Plasmas*
[29]. Halpern F.D. *et al.* 2008 *Physics of Plasmas* **15** 012304 doi:10.1063/1.2829762
[30]. Kinsey J.E. *et al.* 2005 *Physics of Plasmas* **12** 062302 doi:10.1063/1.1920327
[31]. Weiland J. *et al.* 1992 *Nuclear Fusion* **32** 151–155
[32]. Snyder P.B. *et al.* 2001 *Physics of Plasmas* **8** 744–749 doi:10.1063/1.1342029
[33]. Chen Y. *et al.* 2003 *Nuclear Fusion* **43** 1121–1127
[34]. Jenko F. *et al.* 2001 *Plasma Physics and Controlled Fusion* **43** A141–A150
[35]. Candy J. 2005 *Physics of Plasmas* **12** 072307 doi:10.1063/1.1954123
[36]. Takizuka T *et al.* 2006 *Plasma Physics and Controlled Fusion* **48** 799–806

Parameter	**ASDEX Upgrade**	**DIII-D**	**JET**
N	376	103	149
I (MA)	0.6-1.2	1.1-1.3	1.1-2.8
B (T)	1.4-2.8	1.7-1.9	1.4-3.5
q_{95}	3.1-6.2	4.0-5.0	2.7-4.6
$\overline{n}_e$ (10^{19} m^{-3})	3.4-11.4	2.7-7.2	2.0-8.5
P (MW)	2.7-17.1	4.4-11.1	3.7-21.4
$\beta_{N,MHD}$	1.2-3.5	2.2-3.5	1.0-3.5
$\beta_{N,th}$	1.0-3.1	1.8-2.7	0.7-2.6
τ_E (ms)	40-230	80-220	90-390
$H_{98(y,2)}$	0.8-2.0	1.0-1.8	0.7-1.2

Table 1: The number of data points, β_N, and the ranges of key parameters for the ASDEX Upgrade, DIII-D and JET Hybrid scenario dataset of Section 3.

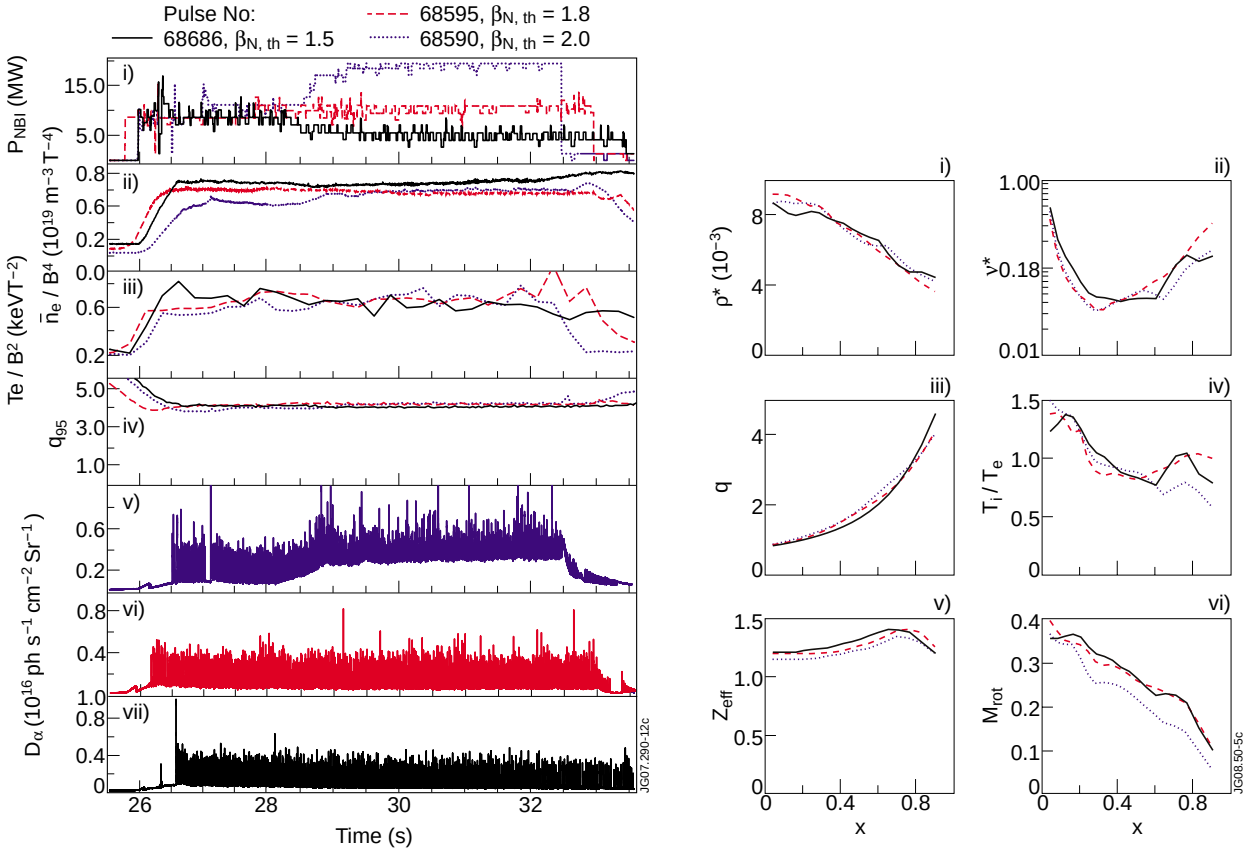

Figure 1: Matches for the three JET β scan discharges: Pulse No's: 68590 (dotted), 68595 (dashed) and 68686 (solid). (a) Time traces of: i) injected NBI power (MW); ii) normalised line average density ($10^{19} m^{-3} T^{-4}$); iii) normalised volume average electron temperature ($keV\ T^{-2}$); iv) q_{95}; and D_α emission from the outer divertor for v) Pulse No's: 68590, vi) 68595 and vii) 68686 (10^{16} $photons^{-1} cm^{-2} sr^{-1}$). (b) Profiles, versus x, of: i) ρ (10^{-3}); ii) ν*; iii) safety factor; iv) ion to electron temperature ratio; v) Z-effective; and vi) normalised toroidal ion Mach number. Time points chosen are: Pulse No's 68590, t=29.5s; 68595, t=29.5s, 68686, t=27s.*

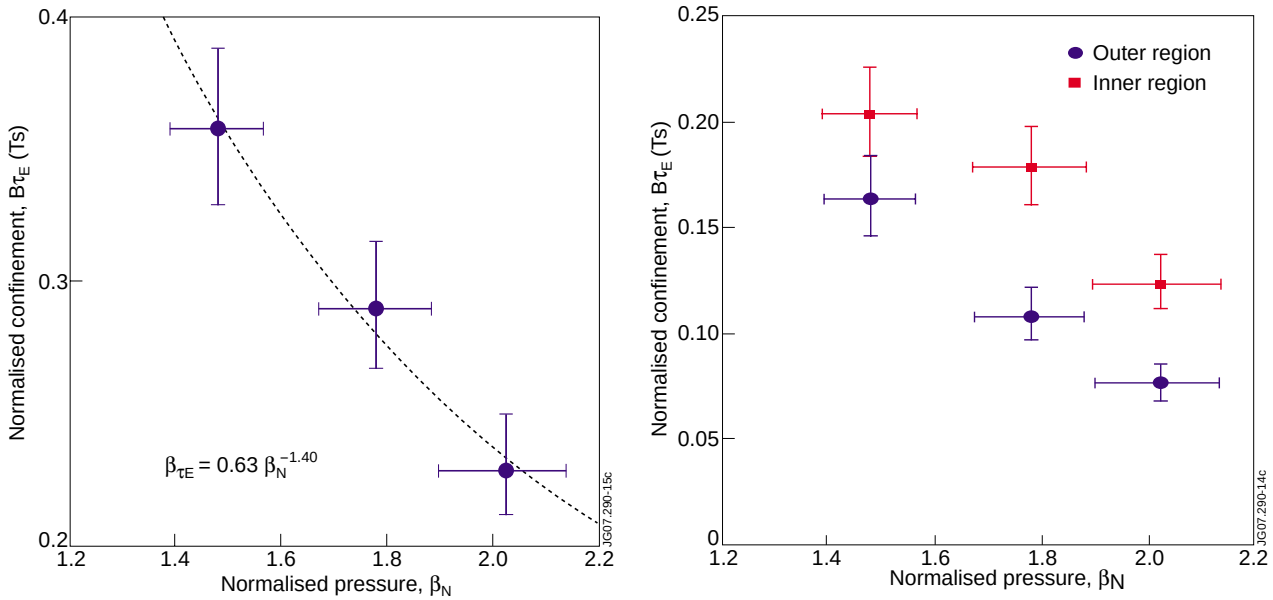

Figure 2: Normalised confinement time, $B\tau_E \propto \omega_{ci}\tau_E$, (Ts) versus normalised global pressure, β_N, for the discharges of figure 1: a) global confinement time; b) an effective confinement time of an inner (circles) region, x = 0–0.8, and an outer (squares) region, x = 0.8–1.0. x is the normalised square root toroidal flux.

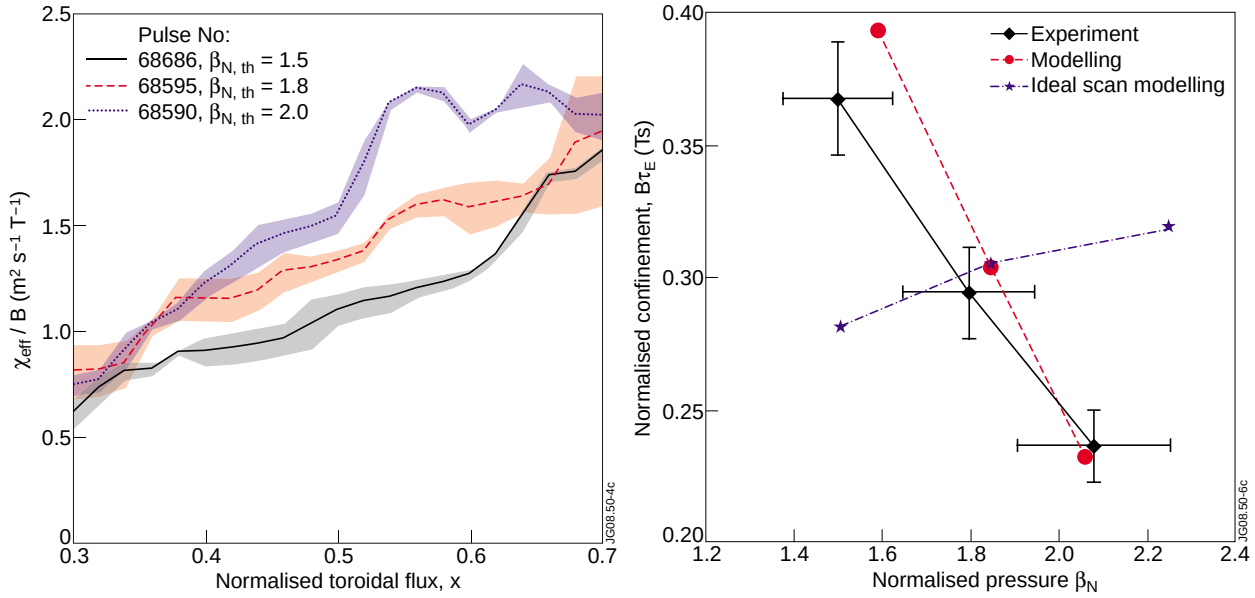

Figure 3: (a) Normalised effective thermal conductivity versus normalised square root toroidal flux, x, for the discharges of figure 1. (b) Normalised confinement, $B\tau_E \propto \omega_{ci}\tau_E$, versus β_N for the same discharges. The confinement is averaged over the region from x = 0–0.8. The diamonds denote the experimental results. The other symbols denote the results of thermal modelling with the Weiland model taking all other parameters from: 1) the central point of the experiment and scaling them as for an ideal beta scan (asterisks) and 2) directly from the experiments (circles).

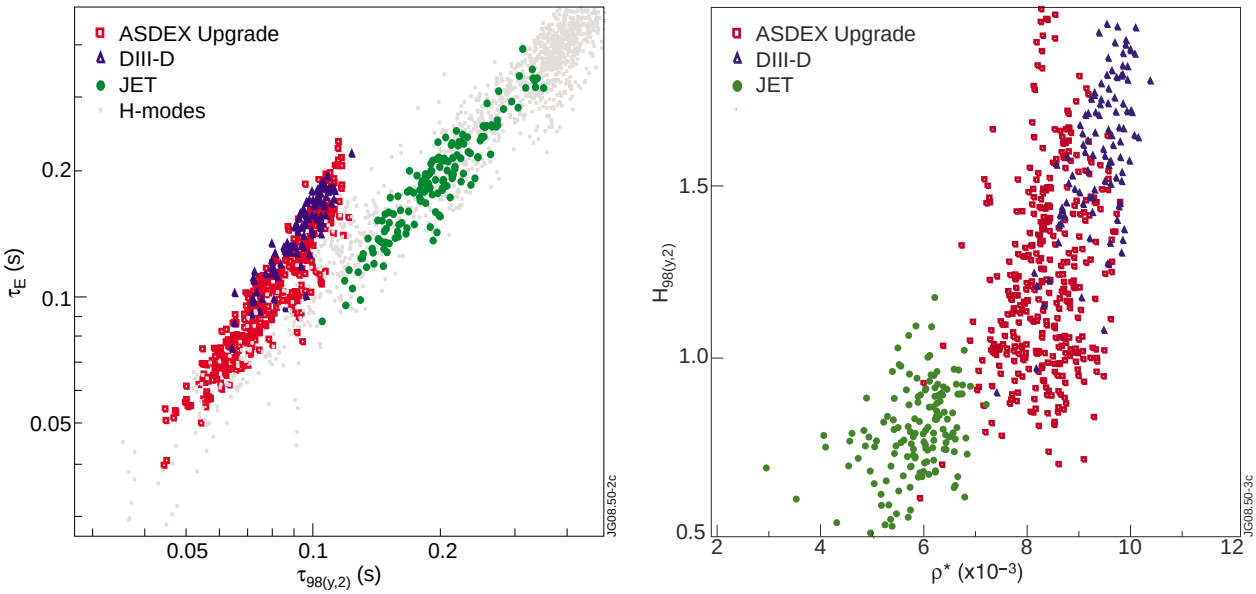

Figure 4: (a) Confinement time (seconds) versus the IPB98(y,2) scaling (seconds) for discharges from the ITER-like standard set of the ITPA H-mode global confinement database (crosses) and the ASDEX Upgrade (squares), DIII-D (triangles) and JET (circles) Hybrid scenario dataset of Section 3. (b) Confinement time normalised to the IPB98(y,2) scaling versus global ρ^* for the Hybrid scenario dataset.